Simulation-based Building Change Detection from Multi-Angle SAR Images and Digital Surface Models

Junyi Tao, Stefan Auer

***Abstract*—This paper presents two change detection strategies based on the fusion of scene knowledge and two high resolution SAR images (pre-event, post-event) with focus on individual buildings and facades. Avoiding the dependence of the signal incidence angle, the methods increase the flexibility with respect to near-real-time SAR image analysis after unexpected events. Knowledge of the scene geometry is provided by digital surface models, which are integrated into an automated simulation processing chain. Using strategy 1 (based on building fill ratio; BFR), building changes are detected based on change-ratios considering layover and shadow areas. Strategy 2 (based on wall fill position; WFP) enables one to analyze individual facades of buildings without clear decision from strategy 1, which is based on a geometric projection of facade layover pixels. In a case study (Munich city center), the sensitivity of the change detection methods is exemplified with respect to destroyed buildings and partly changed buildings. The results confirm the significance of integrating prior knowledge from digital surface models into the analysis of high resolution SAR images.**

***Index Terms*—Synthetic Aperture Radar, Change Detection, Simulation, Urban Areas, Digital Surface Model, TerraSAR-X, High-resolution Imaging, Ray Tracing**

I. Introduction and Motivation

Synthetic Aperture Radar (SAR) satellites are a steady and reliable source of information for object monitoring, and are independent of day and weather. High resolution sensors such as TerraSAR-X/TanDEM-X [1] or Cosmo-SkyMed [2] enable the monitoring of individual targets, e.g., man-made objects such as buildings, bridges or vessels. In the context of buildings, the side-looking concept of SAR sensors favors the analysis of facade structures, which are often represented by salient signatures in the imagery [3]. Prominent SAR image signatures are important in the context of feature extraction [4], [5], radargrammetry [6], interferometry [7], and tomography [8]. The building information extracted from SAR imagery is complementary to information from nadir-looking optical sensors, as exemplified in [9]. In urgent situations, however, the availability of optical sensors may be restricted by clouds and time of day. This limitation may also hamper change detection strategies when integrating optical and SAR data, as is proposed in [10]–[13]. Then, the post-event data base has to rely on SAR. However, due to distortion effects related to the radar imaging concept, the visual or automatic interpretation of SAR images is challenging [14].

Given two SAR images with the same imaging geometry, changes can be detected on a pixel-to-pixel basis or by using more elaborate strategies [15], [16]. In case of sudden events, however, the limitation to equal imaging geometries may contradict with the necessity to analyze the first available post-event SAR acquisition (whose imaging geometry may be different from the one of the pre-event SAR image).

Flexibility with respect to the signal incidence angle reduces the time between comparable data (e.g. from 11 days to less than 3 days for TerraSAR-X), and thereby is likely to also reduce the latency time for change detection results. As a further challenge, the high resolution of modern SAR sensors demands the assignment of changes to individual building structures [17], [18]. The assumption of isolated rectangular buildings is, however, a severe limitation for this task. The integration of 2D vector data from geoinformation systems (GIS) enables one to estimate change ratios for building blocks [19]. However, additional height information is required to predict the outline of elevated objects in SAR images.

Simulation methods implement the integration of 3D knowledge for scenes of interest. As an example, a strategy for georeferencing simulated and real SAR images in the context of building change detection is reported in [20]. The georeferencing is based on extracted line features followed by the manual interpretation of scene changes. Brunner et al. [17] present an algorithm for automatic change detection where simulated and real SAR images are compared based on mutual information. Method limitations are related to the assumption of an isolated rectangular building (box shape) and the manual extraction of building parameters in pre-event optical data for defining the model. Wang and Jin [21] propose a similar concept where different buildings states are simulated and analyzed, i.e., unchanged, collapsed, subsided, or deformed.

Addressing the limitations identified above, this paper contributes the following new aspects:

- Two strategies for change detection (for buildings and facades) based on SAR images captured with different signal incidence angles. The analysis is supported by geometric prior knowledge from digital surface models (DSMs) and extendable to other 3D input formats.
- The detection of changes in the framework of a fully automatic processing chain without the need for manual interaction and co-registration.

Manuscript received Month, Day, Year: revised Month, Day, Year.

J. Tao was with the Remote Sensing Technology Institute (IMF), German Aerospace Center (DLR), Oberpfaffenhofen, Germany, e-mail: junyi.tao@mytum.de

S. Auer is with the Remote Sensing Technology Institute (IMF), German Aerospace Center (DLR), Oberpfaffenhofen, Germany, e-mail: stefan.auer@dlr.de

- A simulation strategy for integrating geometric scene knowledge into an object-based change detection that considers global (e.g. intensity distributions) and local scene properties (e.g. object occlusions).

The methodology is evaluated with respect to reference data for a test scene in the city center of Munich, Germany. The results indicate the gain of prior knowledge from DSMs for change detection methods based on SAR image data. The experiment shows that not only completely demolished buildings but also partly demolished buildings can be detected.

The remainder of the paper is organized as follows. Section II introduces the segmentation and simulation steps required prior to the change detection analysis. Thereafter, two strategies for automated change detection are presented in section III. These strategies rely on the analysis of pixels in building layover and shadow areas. The method application is exemplified by a case study in section IV, which is then followed by a general discussion in section V. Finally, section VI provides a summary of the presented content and an outlook to future enhancements of the methods.

II. Modeling and Simulation

The algorithms for change detection rely on segmentation and simulation steps, which are introduced in this section. The segmentation step is necessary to generate input models, i.e., DSM parts representing the full set of buildings, individual buildings or building walls. GeoRaySAR, the processing chain for SAR simulation, integrates the object geometry into the SAR image analysis in order to enable the automatic scene interpretation.

A. DSM Segmentation for Defining Building and Wall Models

Based on an input DSM, a normalized digital surface model (nDSM) can be generated using the method described in Arefi et al. [22]. Isolated parts in the nDSM, which exceed a size threshold (e.g., 1000 pixels), are then identified as building models. In that regard, the resulting models may be of compact form but also contain courtyards or even comprise neighboring building blocks. If necessary (see section III-B), the building models are further decomposed into wall segments, which is conducted as follows (see example in Fig. 1):

1) A Sobel filter is applied in order to provide a gradient magnitude image (Fig. 1b) and a gradient direction image (Fig. 1c). Both images are smoothed with a median filter of size 5 x 5.
2) Within the neighborhood (3 x 3 patch) of the pixel with the highest gradient magnitude, a height threshold value is calculated (average of the maximum and minimum height in the window).
3) Height values above the threshold are identified (Fig. 1d) and the building boundary polygons (width: 1 pixel) are defined. Depending on the model, the boundaries describe the building outlines, courtyards, or walls of different building blocks.
4) Gradient directions are analyzed along the boundary polygons. A gradient variation above 30° is used as an indicator for building corners where the boundary is split into boundary segments (Fig. 1e; width: 1 pixel). The boundary segments are broadened using a dilation command (width: 3 pixels). As a result, wall masks are obtained.
5) Finally, the wall masks are merged to a wall map (Fig. 1f) where pixels related to a wall model are represented by a dedicated integer value. Furthermore, the median gradient direction and the position of the wall center point are stored for the change detection analysis.

Both segmentation steps are related to limits. Small buildings with little height will be missed in the building segmentation. Similarly, the use of a height threshold in wall segmentation will lead to the loss of low building parts. However, the spatial resolution of the SAR sensor is most crucial in this context, i.e. the number of representative image pixels per object.

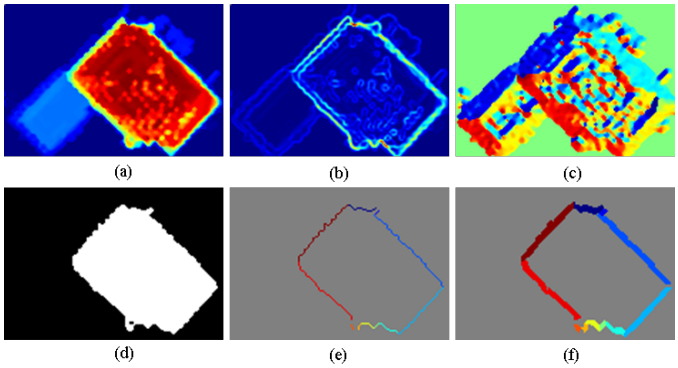

Fig. 1: Extraction of wall models from building model: (a) DSM, (b) gradient magnitude map, (c) gradient direction map, (d) mask based on height threshold, (e) boundary segments, (f) wall mask where colors indicate different walls.

B. Simulation Procedure

The integration of simulation methods into the processing chain enables the identification of scene objects. Accordingly, changes can be assigned to individual objects (see section III). Moreover, a pixel-to-pixel or window-to-window comparison is obsolete, as image parts pertinent to buildings can be analyzed independent to the signal incidence angle. To this end, the geometric information of the DSM and the TerraSAR-X images are fused in the framework of a SAR simulation processing chain (GeoRaySAR [23]). Its core element is RaySAR [24], a SAR simulator based on ray tracing. GeoRaySAR provides geocoded simulated SAR images to be directly superimposed on TerraSAR-X images without a matching step. The simulation relies on scene models with absolute coordinates and orbit parameters defining the sensor perspective (incidence and heading angle).

It should be noted at this point that RaySAR may be substituted with alternative SAR image simulators (e.g. [25], [26]). The latter concept may even allow for real-time processing as it is implemented on a graphics card. GeoRaySAR provides simulation results within several minutes for a given scene model.

DSMs with pixel values related to heights do not represent structural details of building walls. Therefore, the simulation is

restricted to reflection levels 1 (image layer 1: direct response) and 2 (image layer 2: double reflection). To some extent, image layer 2 is also representative for signal triple reflections that are mapped to the bottom end of building walls (see [27] as an example). After DSM segmentation (result: building or wall models), the image layers are simulated for the respective DSM, DTM (digital terrain model without elevated objects), and nDSM (normalized digital surface model containing elevated objects). Masks for double reflection, building layover, building shadows, background without image content, and ground parts are generated by a combination of the layers (see [23] for details).

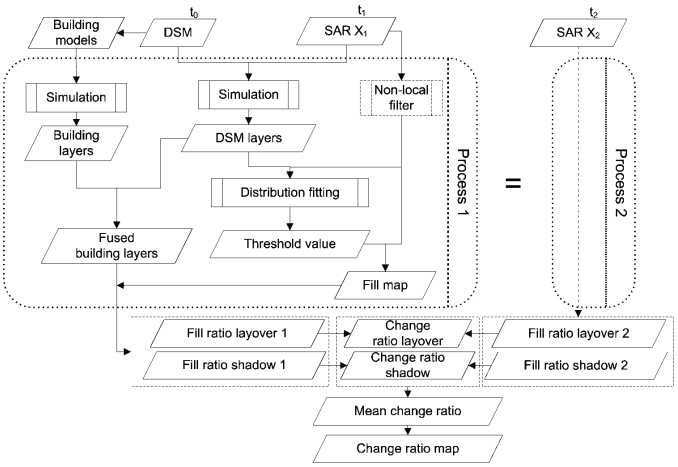

Fig. 2: Change detection based on building fill ratio (BFR; non-local filtering as optional component).

(a) TerraSAR-X image

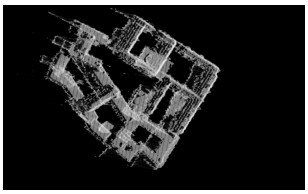

(b) Simulated image

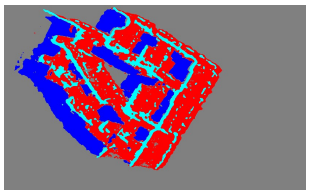

(c) Fused layers considering occlusions of nearby buildings (blue: shadow, red: layover, cyan: double bounce, grey: background)

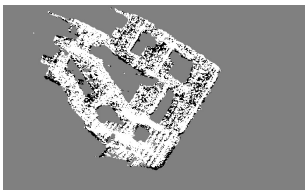

(d) Fill map of building layover layer (white: value above threshold, black: value below threshold, grey: background without information)

Fig. 3: Example: Generation of fill map; building in Munich city center.

III. Methods for Change Detection

A. Change Detection based on Building Fill Ratio (BFR)

In case of a demolished building, signal responses from its facade and roof structures will disappear while the signal response from its former shadow area will increase due to removed occlusions. The former layover area will mostly contain signal responses from the ground in front of the building. Accordingly, the change detection task relates to the separation of signal responses of the building layover / shadow from that of the ground.

The task may be solved by exploiting geometric or radiometric features of the building in the SAR image such as corner lines [28], the L-shape geometry of buildings [4], or line signatures related to building layover and shadows [29]. However, these concepts are adapted to specific building types, e.g., isolated rectangular buildings. Moreover, the extraction of features and their assignment to individual buildings may fail for scenarios with dense settlements, where nearby buildings overlap in the SAR image.

Instead of image features, the intensity distributions of SAR image pixels related to building layover / shadow and ground are analyzed based on simulated image layers in the BFR method. Two high resolution SAR images (X_1 and X_2), acquired with different incidence angles for the same geographical area at different times (t_1 and t_2), represent the pre- and post-event status of the scene. Optionally, the images can be de-noised by a non-local filter (see [30]; no iteration) prior to the processing, which slightly improves the identification of changes at the cost of additional processing time (20 minutes for the test scene analyzed in section IV). Moreover, a DSM is available for time point t_0, which is earlier than or equal in time to t_1. It is assumed that only few of the buildings have been demolished between time points t_1 and t_2. The aim is to detect building-related changes with independence of the signal incidence angles. Fig. 2 shows the flowchart of the algorithm which contains the main processing steps:

1) Based on the DSM, image layers are generated for each building using GeoRaySAR (see section II-B) for layover, double-bounce, shadow and ground. In this context, occlusions between scene objects are considered (fused building layers).
2) Based on these layers, two threshold values are calculated for separating building and shadow pixels from ground pixels, respectively.
3) Applying the defined thresholds, two binary images, referred to as fill maps, are generated from the SAR image. The fill maps represent the intensity distribution of the full scene.
4) The fused building layers are superimposed on the fill maps in order to calculate the fill ratios of building layover and shadow areas.
5) Steps 1-4 are repeated for SAR image X_2.
6) The fill ratios derived from both SAR images are compared for each building in order to obtain a change ratio for layover and shadow.
7) The mean change ratio is calculated for each building and used as an indicator for demolished buildings.

The strategy aims at the ability to compare two SAR images with varying signal incidence angles as well as the special case of equal signal incidence angles. The key processing steps of

the procedure are detailed in the following.

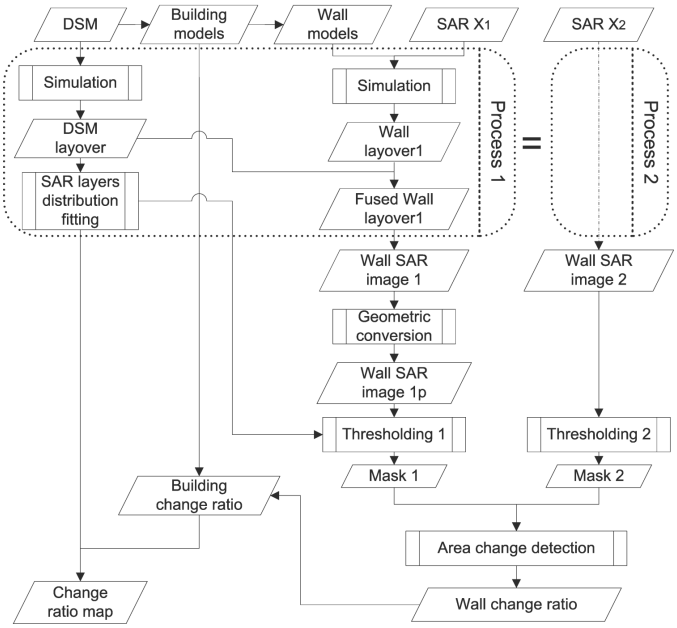

Fig. 4: Change detection based on wall fill position (WFP).

1) Threshold definition: From SAR image X_1, image pixels can be identified by means of the simulated layers for layover (image pixels X_{1l}), shadow (X_{1s}), and ground (X_{1g}). Pixels belonging to the double-bounce layer are also included in X_{1l}. Intensities are analyzed in logarithmic scale based on the assumption that logarithmically scaled intensities of urban clutter and building layover are normally distributed (see [31] and [32]). The assumption of normal distribution also roughly applies to logarithmically scaled intensities of building shadow, which is often a mix of true shadow and signal multiple reflections [33].

Following the assumption of normal distributions, the distribution of X_{1s} and X_{1g} are approximated by Gaussian functions:

$$f(x) = \frac{1}{\sigma_m\sqrt{2\pi}} \exp\left\{-\frac{(x-\mu_M)^2}{2\sigma_M^2}\right\} \sim N\left(\mu_M, \sigma_M^2\right) \quad (1)$$

with $M \in \{1l, 1s\}$. The equation components μ_M and σ_M^2 are the mean and variance of the distributions, respectively. Based on the Bayesian decision rule, a threshold value T_{1lg} is calculated for separating layover and ground pixels. Similarly, the threshold value T_{1sg} is derived for separating shadow and ground pixels.

Preferably, no building changes should have happened between the time stamps related to the DSM and pre-event SAR image, which is usually not the case. However, if only a small number of buildings have changed between t_0 and t_1, the threshold values remain appropriate for subsequent steps.

2) Calculation of fill ratios: Two binary images F_{1lg} and F_{1sg} are derived by applying the thresholds T_{1lg} and T_{1sg} to the SAR image ("fill maps"). Therein, value 1 in F_{1lg} indicates pixels with intensities higher than T_{1lg}, whereas value 1 in F_{1sg} indicates pixels with intensities lower than T_{1sg}.

Layover and shadow layers are generated for the whole DSM and for each building using GeoRaySAR (see section II-B). Object occlusions are considered by overlapping the global (DSM) layers with the local building layers and thus resulting in the fused building layover and its area A_l. By applying the threshold criterion to the intensities in the fused building layover, the corresponding fill area is obtained (A_{lf}; number of pixels with value 1). For image X_1, the fill ratio related to the layover of a building is then

$$r_{1l} = \frac{A_{1lf}}{A_{1l}} \quad (2)$$

which is considered as an indicator for the amount of man-made structures within the layover. As an example, the fused layers and the fill map of a building are shown in Fig. 3.

Correspondingly, the fill ratio of building shadow is defined as

$$r_{1s} = \frac{A_{1sf}}{A_{1s}} \quad (3)$$

where A_{1sf} is the area covered by pixels fulfilling the threshold criterion and A_{1s} the full area of the shadow layer. Equally, the fill ratios r_{2l} and r_{2s} are derived for SAR image X_2.

3) Calculation of Change Ratio: Change ratios are calculated based on the fill ratios. For the building layover, the ratio

$$P_l = max\left\{1 - \frac{r_{2l}}{r_{1l}}, 0\right\} \quad (4)$$

aims to detect demolished buildings (positive changes with $r_{2l} > r_{1l}$ are discarded). In order to avoid the following fusion steps from being misled, negative values of P_l are modified to 0. Destroyed buildings are indicated by high values of P_l. Similarly, the change ratio of the building shadow is

$$P_s = max\left\{1 - \frac{r_{2s}}{r_{1s}}, 0\right\} \quad (5)$$

Combining the ratios of layover and shadow, the mean change ratio of the building is

$$P_b = \frac{P_l A_{1l} + P_s A_{1s}}{A_{1l} + A_{1s}} \quad (6)$$

where the area of layers is considered as weights.

B. Change Detection based on Wall Fill Position (WFP)

The BFR method described above enables the ability to detect fully demolished buildings. Partly demolished buildings, however, are expected to lead to unclear decisions due to changed and unchanged parts merged within the same layover and shadow layers. Concentrating on such situations, the WFP method has been developed to analyze changes of individual walls.

Again, the analysis is based on a given DSM and two SAR images captured at times t_0, t_1 and t_2, respectively, with the focus being set on negative changes between time points t_1 and t_2. This time, the analysis concentrates on facade layover only. The WFP method is characterized by the following steps (see flowchart in Fig. 4):

1) Individual walls are extracted from the DSM (see section II-A), followed by the simulation of image layers for the wall models and the DSM.

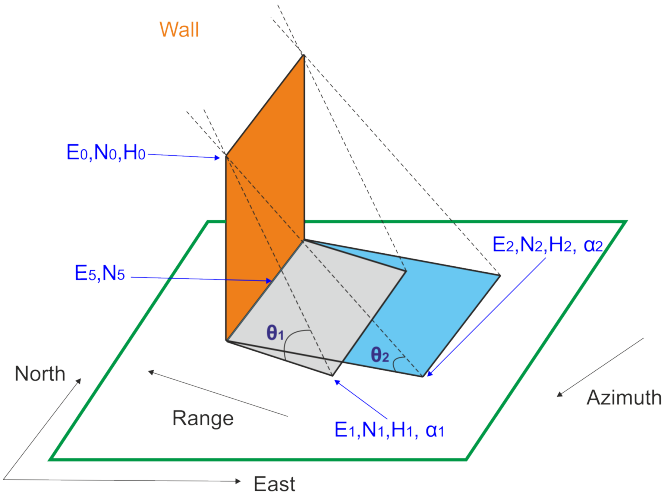

Fig. 5: Geometry related to the conversion of facade layover pixels.

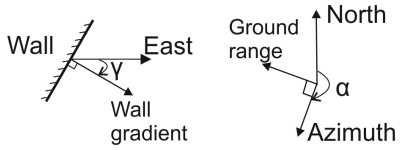

Fig. 6: Azimuth angle α and wall gradient direction γ for calculating aspect angle Φ.

2) Fused layover layers are generated for each wall where occlusions due to nearby buildings are considered.
3) The layover image patch from X_1 is transformed to meet the imaging geometry related to image X_2 (see details below).
4) From both layover image patches, fill maps (F_{1lg}, F_{2lg}) are obtained based on intensity thresholds (compare section III-A1).
5) The change ratio is calculated for each building wall based on the position of pixels fulfilling the threshold criterion.
6) Finally, the wall change-detection results are fused on a building-level to calculate the building change ratio.

Again, it has to be noted that this strategy is also applicable to SAR images captured with equal signal incidence angle. Under such conditions, no geometric layover conversion is required. Details on the wall layover conversion and change detection strategy are provided next.

1) Wall layover conversion: The principle of wall layover conversion (see Fig. 5) follows the assumption of vertical and planar building walls. The basic idea is to project a layover pixel from SAR image X_1 to a point on the vertical plane (projection 1) and then into the image plane of SAR acquisition X_2 (projection 2). To begin, the known parameters for the projection step are

- Point P_1 with coordinates (E_1, N_1) in the wall layover of SAR image X_1 .
- Signal incidence angles, azimuth angles and frame mean heights of the two SAR images (θ_1, α_1, H_1, θ_2, α_2, H_2)
- Wall gradient direction (ω), wall center point P_5 with coordinates (E_5, N_5), both provided by the DSM segmentation (see section II-A).

The aim is to calculate the coordinates E_2, N_2 of the corresponding point P_2 in SAR image X_2. Considering the imaging geometry, the correspondence of a wall point P_0 with coordinates E_0, N_0, and H_0 and the two points in both SAR images can be described as

$$\begin{pmatrix} E_0 \\ N_0 \\ H_0 \end{pmatrix} = \begin{pmatrix} E_1 \\ N_1 \\ H_1 \end{pmatrix} + \lambda_1 \begin{pmatrix} cos\alpha_1 \\ -sin\alpha_1 \\ tan\theta_1 \end{pmatrix} = \begin{pmatrix} E_2 \\ N_2 \\ H_2 \end{pmatrix} + \lambda_2 \begin{pmatrix} cos\alpha_2 \\ -sin\alpha_2 \\ tan\theta_2 \end{pmatrix} \tag{7}$$

The point P_0 is situated on the vertical plane, leading to the equation

$$\begin{pmatrix} cos\omega \\ -sin\omega \end{pmatrix} * \begin{pmatrix} E_0 - E_5 \\ N_0 - N_5 \end{pmatrix} = 0 \tag{8}$$

Taking the first two lines of equation 7 and substituting E_0 and N_0 in equation 8, we derive

$$\begin{aligned} \lambda_1 &= \frac{cos\omega\,(E_5 - E_1) + sin\omega\,(N_1 - N_5)}{cos\,(\omega - \alpha_1)} \\ \lambda_2 &= \frac{H_1 - H_2 + \lambda_1 tan\theta_1}{tan\theta_2} \\ E_2 &= E_1 + \lambda_1 cos\alpha_1 - \lambda_2 cos\alpha_2 \\ N_2 &= N_1 - \lambda_1 sin\alpha_1 + \lambda_2 sin\alpha_2 \end{aligned} \tag{9}$$

to project layover pixels between the SAR image planes. The error of the projection is primarily related to the appropriateness of the flat plane assumption. The impact of the error is limited for the change detection algorithms presented in this paper, as that the analysis relies on region-based image properties.

2) Selection of proper walls: The wall segmentation described in section II-A has provided wall models with geometric properties (height, median gradient direction, length). Not all walls are visible to the SAR sensor. Given a wall with gradient direction γ and the azimuth angle α related to the sensor (see Fig. 6), the aspect angle

$$\Phi = |\gamma + 180^\circ - \alpha| \tag{10}$$

is the angle between the wall normal direction, i.e. the gradient direction derived from the wall segmentation (see section II-A), and the range direction of the sensor projected on the ground. The aspect angle ranges between 0° and 180°. If the wall is oriented parallel to the line-of-flight, the aspect angle is 0° and the wall layover area is maximal in the SAR image. The increasing aspect angle narrows the layover area in the azimuth direction, and thereby causes the separation of salient signatures to become more and more difficult. Walls with aspect angles bigger than 90° are outside the field-of-view of the SAR sensor. The specified scene only considers only walls with aspect angles smaller than 85° for the analysis.

3) Detection of Wall Changes: For each building, the SAR image patch related to a wall in X_1 is projected to the geometry of SAR X_2 following the description in section III-B1. Subsequently, the converted image is re-sampled with bi-cubic interpolation. Equal to the BFR method, two (binary) fill maps (F_{1lg} and F_{2lg}) are generated marking representative layover and ground pixels in the corresponding areas. The therefore required two thresholds are derived from the DSM layers (see section III-A1). The change ratio is calculated based on the fill maps. In contrast to the BFR method, not only is the amount of representative pixels analyzed but also their position.

The filled area (number of pixels with value 1) in mask F_{1lg} is defined as A_{1lf}. Moreover, the intersecting area between the fill maps F_{1lg} and F_{2lg} with value 1 in both maps is defined as A_{1lfi}. The change ratio based on the position of layover fill is then

$$P_w = 1 - \frac{A_{1lfi}}{A_{1lf}} \tag{11}$$

As a final step, change ratio results of n individual walls can be merged into a joint building change ratio, considering the area A_{1lf_k} of wall number k as weight. The resulting change ratio

$$P_b = \frac{\sum_{k=1}^{n} P_{w_k} A_{1lf_k}}{\sum_{k=1}^{n} A_{1lf_k}} \tag{12}$$

can be used as an indicator for building changes, which may allow for a more direct analysis than individual change ratios on the wall level.

Change time	$t_2 - t_1$					$t_1 - t_0$	
New	N2	N4	N5	N6		N1	N3
Building ID	9*, 19*	75*, 70*	77*, 79*	78*		9*, 12*	33*, 40*
Rebuilt	R6	M1	R1	R2	R5	R3	R4
Building ID	76 (L)	22 (M)	44 (S)	7 (S)	24 (S)	19 (L)	33 (L)
Demolished	D1	D2	D3				
Building ID	26 (L)	75 (L)	59 (S)				

TABLE I: Correspondence between visually identified changes (polygons) related to $t_2 - t_1$ and $t_0 - t_1$ (Fig. 9) and the IDs of building models extracted from the DSM (Fig. 7b). The letters S (mall), M (edium), and L (arge) categorizes the extent of the change (polygon) compared to the full building size. The asterisk * denotes nDSMs of former building models that are located near polygons of newly constructed buildings.

IV. Case Studies

A. Test scenario

In order to test the change detection methods, a case study has been conducted for the Munich city center based on two geocoded high resolution spotlight TerraSAR-X images (without non-local filtering) and a DSM derived from a LiDAR point cloud. The TerraSAR-X images have been acquired on a descending orbit with incidence angles of 25.3° (time point t_1 at 2008-05-26) and 39.3° (time point t_2 at 2010-01-05). The

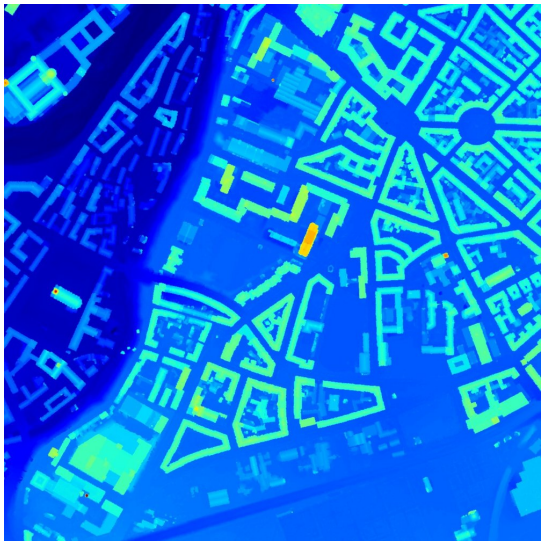

(a) Digital surface model; vertical and horizontal resolution: 0.1 m and 1 m

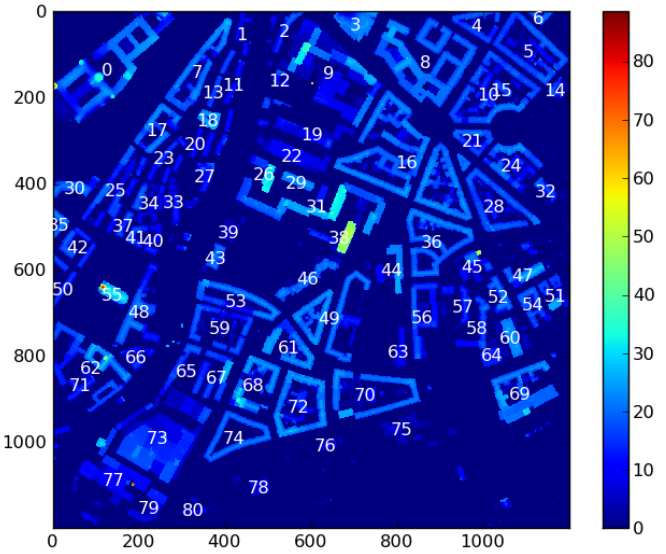

(b) Building IDs derived from segmenting the nDSM

Fig. 7: Scene knowledge based on LiDAR acquisition from April 2003.

LiDAR data have been acquired in April 2003 (time point t_0) with a vertical / horizontal resolution of 0.1 m / 1 m. Vegetation has been removed by a filtering step. Two sub-parts of the DSM have been selected to exemplify the potential of the change detection methods:

- an extended DSM scene for the analysis on the building level (see Fig. 7a), containing several changed buildings, and
- a small DSM scene for the analysis on the wall level (see Fig. 18c), containing one partly changed building.

TerraSAR-X images related to time points t_1 and t_2 are shown in Fig. 8 and Fig. 18, respectively. The spatial resolution of the original SAR images is 1.1 m in azimuth and 0.6 m in range, respectively. The pixel spacing of the geocoded image

Overall accuracy	92.6%	Prediction		Producer's accuracy
Kappa coefficient	0.532	Change	No change	
True	Change {building IDs}	4 {22, 26, 75, 76}	4 {7, 24, 44, 59})	50.0%
	No change {building IDs}	2 {19, 39}	71 {other building IDs}	97.4%
User's accuracy		66.6%	94.7%	

TABLE II: Confusion Matrix; detected buildings and kappa coefficient for the unsupervised change detection based on building layer fill; change ratio threshold for separating "change" from "no change": 0.2, selection based on histogram in Fig. 14.

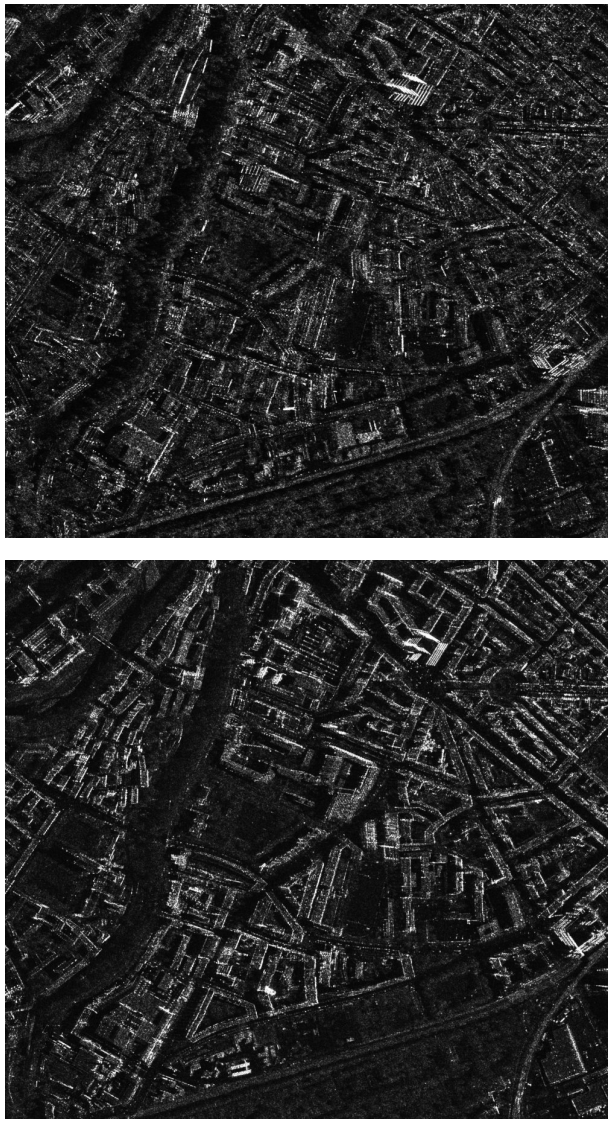

Fig. 8: Geo-coded spotlight TerraSAR-X images of Munich test site (UTM coordinates, range direction: right to left); (top) Image X_1 acquired on 2008-05-26 with incidence angle 25.3°, (bottom) Image X_2 acquired on 2010-01-05 with incidence angle 39.3°. Pixel spacing in east and north: 0.5 m.

is 0.5 m along both axes.

The focus of the case study is on changes between time points t_1 and t_2. In between these time points, buildings might have been demolished or rebuilt. Moreover, object materials might have changed or new buildings might have been constructed. All of these changes affect the appearance of the urban scene in the SAR images. Changes between time points t_0 and t_1 are excluded from the analysis.

As a reference, optical images of Google Earth have been visually analyzed (time points 2007-08-25 and 2009-05-23) to identify apparent changes (see Fig. 9 for large test site and Fig. 19 for small test site). Besides the optical imagery, a third TerraSAR-X image X_3 is available with the same incidence angle as X_1 and a similar acquisition time (2010-01-10) as X_2. For visual inspection, multi-temporal false color composite images of the SAR images X_1 and X_3 are generated (see Figs. 15b and 18d). Therein, the colors magenta and green indicate increased and decreased intensity, respectively.

B. Scene Simulation and Threshold Definition

A total of 81 buildings are derived by segmenting the DSM shown in Fig. 7a. Most of the buildings contain courtyards and have heights of about 30 m (see building IDs in Fig. 7b). As many scene buildings are located close to each other, there exists a large interference of many layover parts of adjacent walls and buildings. Using GeoRaySAR, the layover, shadow and ground image layers are generated for the DSM (see Fig. 10) and for the building models. Based on the DSM layers, intensity distributions are obtained for ground, layover and shadow regions in SAR images X_1 and X_2 (see Fig. 11). Probability density functions (PDFs, see equation 1) are estimated from the histograms of layover, ground and shadow pixels. Black vertical lines in Fig. 11 mark the estimated intensity thresholds to separate ground from layover and shadow. Since SAR image X_2 has been taken with a larger incidence angle than image X_1, signatures inside the facade layover areas are more compressed, and therefore lead to higher intensities. Thus, the threshold for separating ground from layover is slightly higher for image X_2. In contrast, the estimated thresholds for separating shadow and ground are similar. The estimated PDFs for both SAR images show strong overlap but still allow for the separation of both thresholds in logarithmic scale. The impact of the PDF overlap is limited as only the relative fill ratio is compared in the change detection procedure. However, the separability of the PDFs depends on the signal incidence angle, which influences the relative weight between ground and building signal contributions in the layover area (non-linear dependence of the image radiometry). Considering the imaging geometry of a SAR system, small incidence angles are related to a higher amount of (disturbing) ground signals in building layover. Accordingly, the separability of the PDFs is expected to improve for larger signal

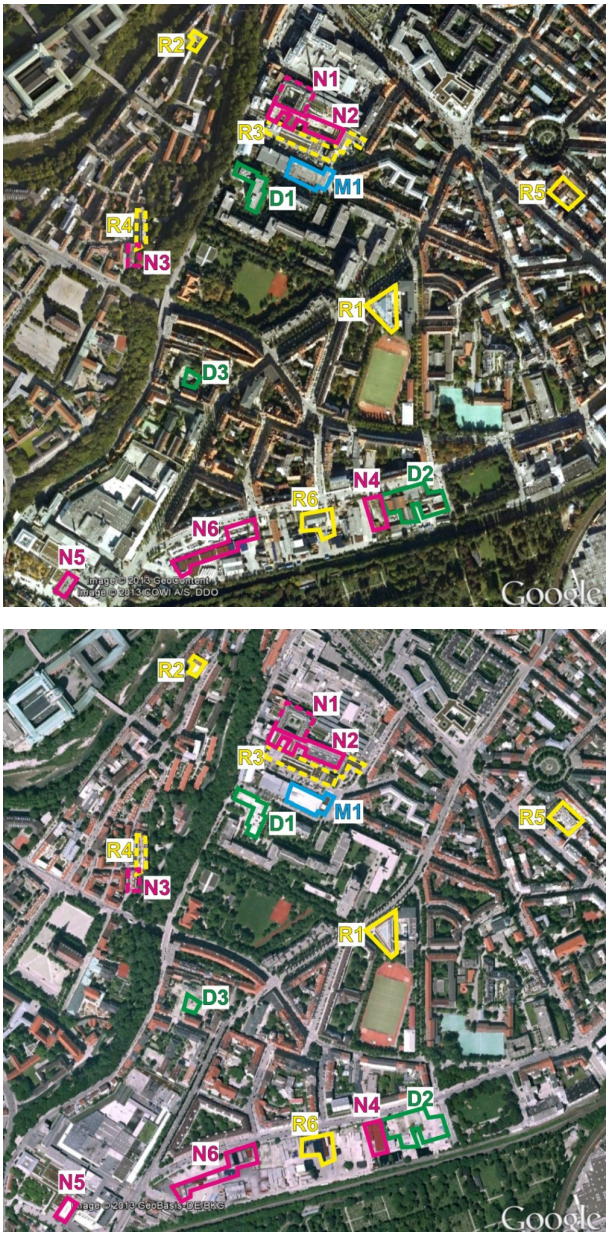

Fig. 9: Apparent changes identified based on visual inspection of Google Earth images. (top) 2007-08-25, (bottom) 2009-05-23. Different types of changes are marked with dashed (changes between t_0 and t_1) and solid (changes between t_1 and t_2) polygons with different colors (magenta: new; green: demolished; yellow: rebuilt; cyan: change of material).

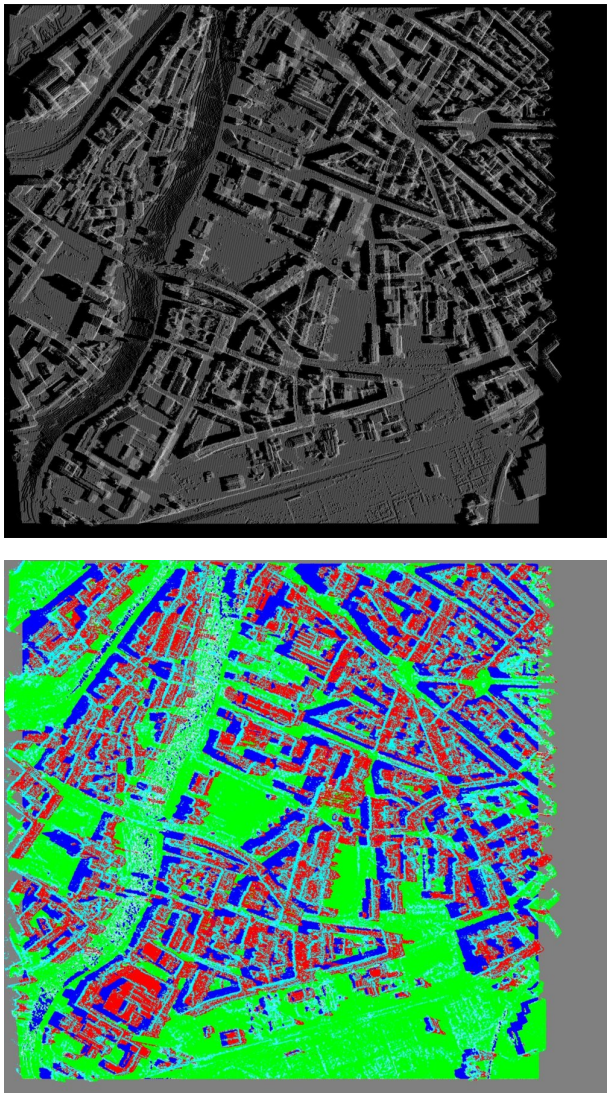

Fig. 10: Simulated image and layers for imaging geometry of SAR image X_1; (top) simulated image, (bottom) separate layers (blue: shadow; green: ground; red: layover; cyan: double reflections; gray: background).

incidence angles (as slightly indicated in Fig. 11).

C. Change detection on building level

The BFR method (see section III-A) is used to analyze changes in the corresponding image layers for all buildings. As a result, the layover fill ratios of these buildings (most range from 0.5 to 0.7) are shown in Fig. 12. The difference to the ideal value 1 is related to the fact that layover areas also contain low intensities (depending on the geometry and material). The fill ratio is a characteristic of the building and allows for analyzing changes to the building appearance.

Fig. 13 shows the change ratios of the buildings based on the layover, shadow, and fused layer (i.e. layover and shadow). Some shadow change ratios are 0 due to the definition of equation 4, while others are even higher than the corresponding values from the layover layers. In comparison, the change ratio of layover areas shows less variation. Fusing the change ratios to the mean change ratio stabilizes the analysis.

The resulting histogram of the mean change ratios of the 81 buildings is shown in Fig. 14. The ratios mostly range from 0.0 to 0.2, which is close to the ideal value 0 for unchanged buildings. Three buildings (IDs: 76, 26, and 75) provide significantly higher change ratios (0.597, 0.584, and 0.461) than the other ones, indicating that they are demolished. Three other buildings (Building 39, 22, 19) correspond to mid-level change ratios ranging between 0.2 and 0.3. Fig. 14 provides a ranking of change ratios where, for instance, threshold 0.2 may be selected for separating ”change” from

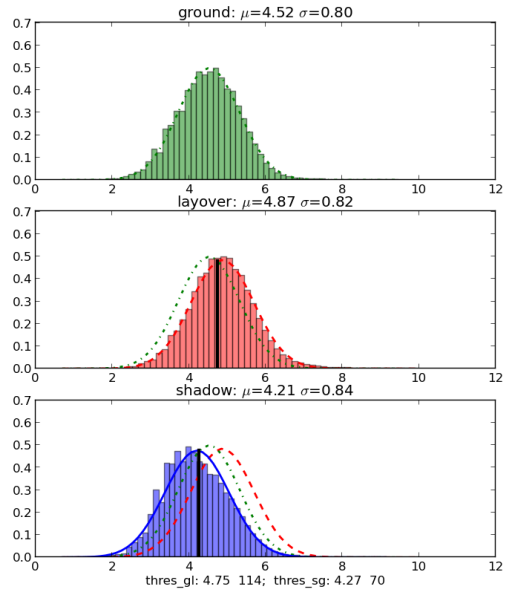

(a) Distributions related to image X_1, date: 2008-05-26, incidence angle: 25.3°

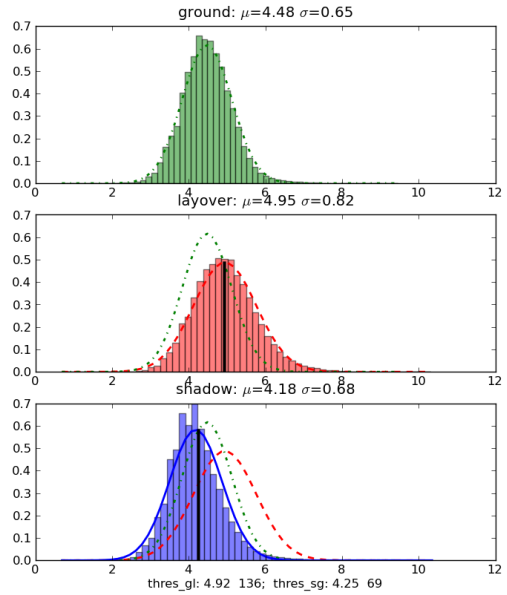

(b) Distributions related to image X_2, date: 2010-01-05, incidence angle: 39.3°

Fig. 11: Threshold definition based on intensity distributions. The estimated PDFs (lines) correspond to the ground, layover and shadow layers of the scene DSM; Black vertical lines mark thresholds for separating ground from layover and shadow; "thresh": thresholds for separating ground from layover (gl) and shadow from ground (sg), followed by the log-value of intensity and intensity.

"no change" based on identifying a gap in the histogram (see also discussion on threshold definition in section V). This option is used for change detection, as will be discussed in the following (see confusion matrix in table II). Alternatively, mid-change ratios may be assigned to a third class, where a subsequent analysis on the facade level may be initiated (see

Fig. 12: Layover fill ratio of the scene buildings (BFR method). The vertical lines mark eight changed buildings which are summarized in Table I. Slightly changed buildings are marked with S after their IDs.

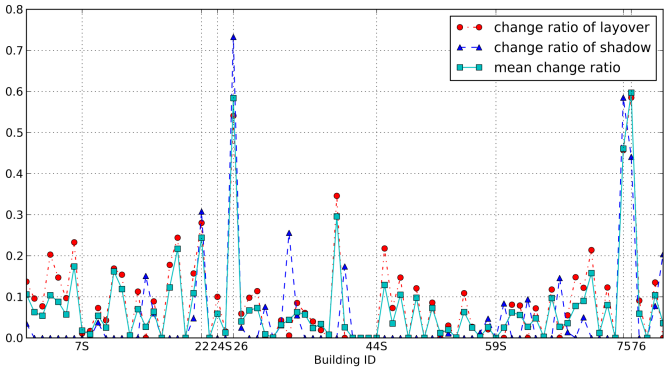

Fig. 13: Building change ratio for layover, shadow and fused layers (layover and shadow) based on BFR method.

section III-B).

The manual identification of apparent changes, summarized in table I, leads to a confusion matrix, which is shown in table II. Most importantly, the totally demolished buildings 26 and 75 are identified. Two further buildings (76 and 22) are assigned with medium change ratios that correspond to medium changes in reality (rebuilt areas). The change related to building 19 is not a false alarm, as that a nearby newly constructed building affects its signal response (see N2 in Fig. 9). In contrast, the change detected for building 39 is a false alarm which presumably results from the seasonal change of adjacent trees that partly occlude the roof of the building. As expected, four buildings with partial changes (IDs: 7, 24, 44, 59) are not detected as the analysis is conducted on the building level.

Fig. 15a visualizes the mean change ratios in a map which correspond to the given scene knowledge (Fig. 9) and the false color composite (Fig. 15b).

A further extension of the incidence angle difference reduces the capability of detecting changes. This is indicated by the processing example shown in Fig. 16 where two incidence angles near the imaging limits of TerraSAR-X are selected (2008-06-27: incidence angle 50°, 2010-01-10: incidence angle 25.3°). As a further variation, the data constellation is

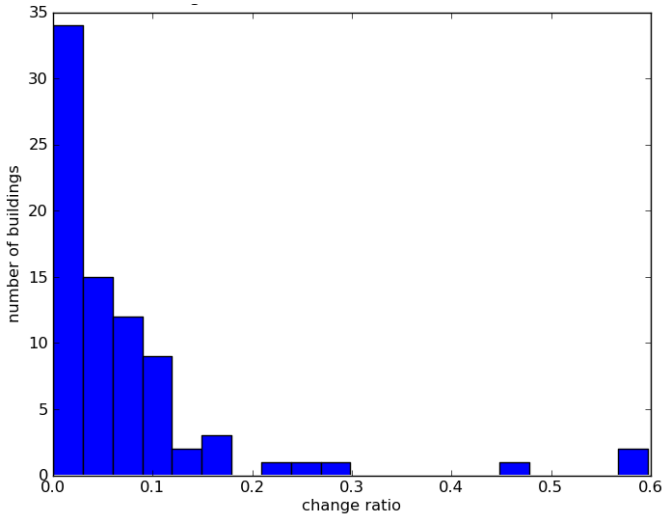

Fig. 14: Histogram of mean change ratios of scene buildings (BFR method). Low change ratios indicate unchanged buildings. The top-five change ratios correspond to buildings 76, 26, 75, 39, and 22 with change ratios of 0.6, 0.58, 0.46, 0.30, and 0.24.

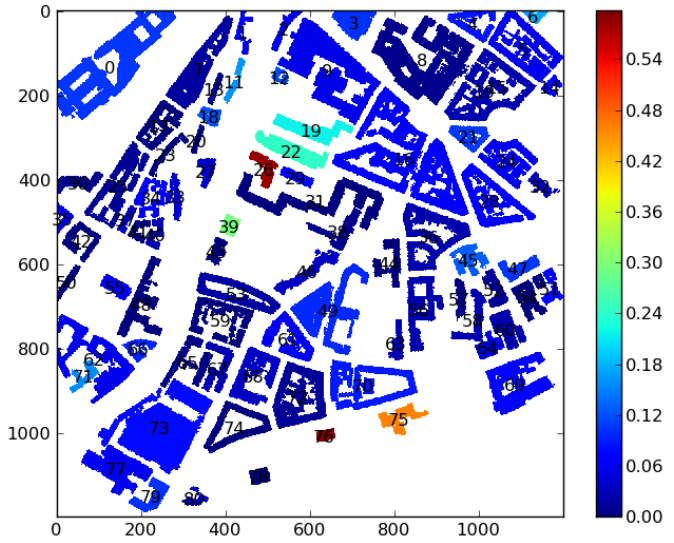

(a) Change ratio map based on BFR method (color indicates the building mean change ratio). Difference between signal incidence angles: 14.0°. Compare Fig. 7b for building IDs.

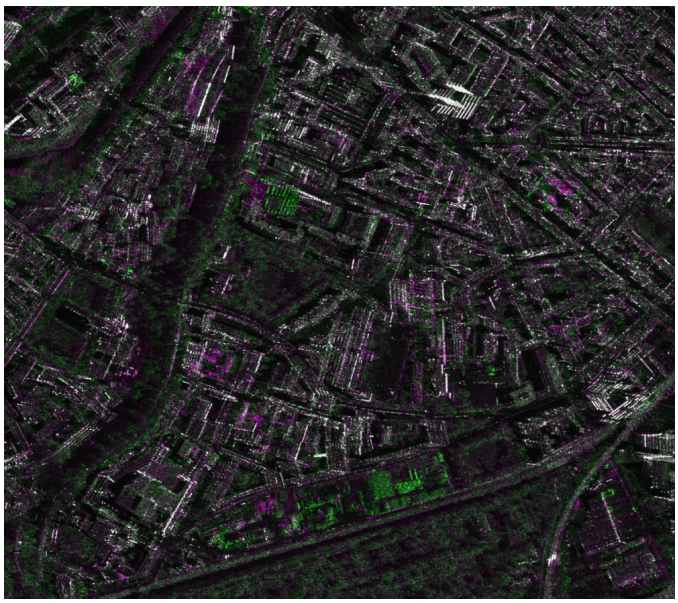

(b) Multi-temporal false color composite of spotlight TerraSAR-X images X_1 and X_3 (Red and blue channel: 2010-01-10, Green channel: 2008-05-26), both captured with incidence angle 25°). Magenta and green indicate increased and decreased intensity.

Fig. 15: Change detection on building level: change ratio map (top) vs. false color composite (bottom).

now changed given that the larger incidence angle is linked to the pre-event situation in 2008. The change ratio map, shown in Fig. 16a, reveals that the change ratio of the demolished building 26 is even higher than the former result (increase from 0.6 to 0.8). Again, the majority of buildings are assigned with low change ratios within the interval between 0 and 0.2 (see Fig. 16b). Above, an extended group is assigned with medium change ratios that occur due to various reasons. Building 13 (change ratio: 0.47) and building 11 (change ratio: 0.44) are likely affected by construction work (see Fig. 17), i.e. roof parts are removed at building 13; vegetation and containers are removed from the ground in front of building 11, which affects the layover area of the building. The increased difference in the layover extent may also be the reason for the medium change ratio 0.34 of building 78. Only objects near the building have changed, i.e. equipment surrounding the building and the adjacent change area N6. Rebuilt building 44 is related to a medium change ratio of 0.36 and is thus separable from unchanged candidates. Building 76 is also assigned to the group of medium change ratios, whereas the change of building 75 cannot be distinguished. A look to the change ratio histogram favors thresholds of 0.2 or 0.4.

Altogether, the processing example indicates that prominent changes can be identified for various incidence angle differences. Nonetheless, using SAR imagery with smaller angle differences is favored as the comparability of layover content is improved (similar geometric extent, impact of adjacent objects, and influence of object occlusions).

Concerning the processing time, the test scene is simulated in less than two hours (Inter Core2 Quad CPU 2.83-GHz, 8-GB RAM, 64-bit Linux operation system CentOS 5.8). The time-demanding part is the simulation of the whole scene and 81 building blocks. As the simulations are conducted sequentially, the processing time may be optimized by parallel computing in future applications.

D. Change detection on wall level

As shown in the last section, the change detection algorithm on the building level (see section III-A) enables one to detect prominent changes. Complementary, the change detection algorithm for individual walls (WFP) may solve the analysis where extended building blocks only partly change. To exemplify this, an example is given below for a smaller test site. The input data (DSM, two SAR images) are shown in Fig.

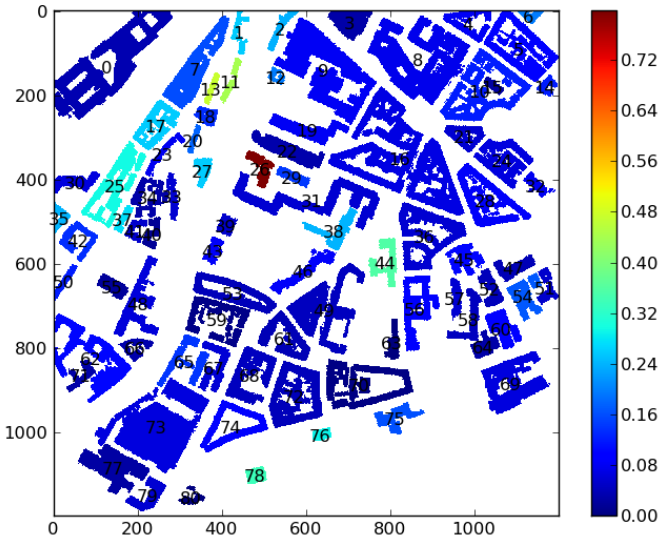

(a) Change ratio map based on BFR method (color indicates the building mean change ratio). Difference between signal incidence angles: 24.7°. Compare Fig. 7b for building IDs.

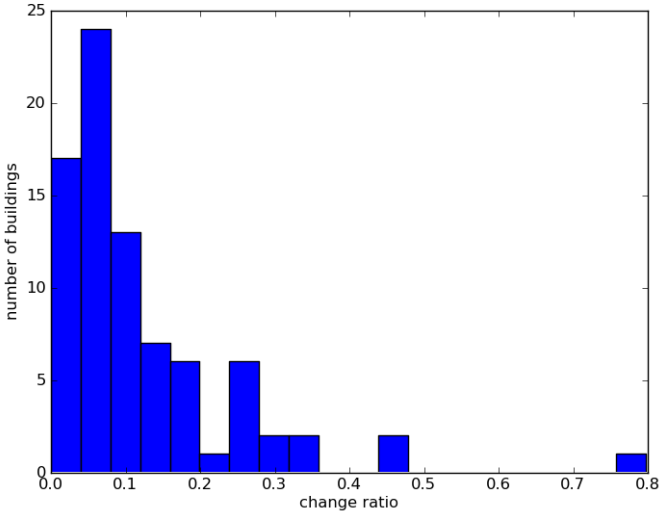

(b) Histogram of mean change ratios of scene buildings. The five highest change ratios correspond to buildings 26, 13, 11, 44, and 78 with change ratios of 0.8, 0.47, 0.44, 0.36, and 0.34.

Fig. 16: Change detection with an extended incidence angle difference (2008-06-27: incidence angle 50°, 2010-01-10: incidence angle 25.3°). Top: change ratio map; bottom: histogram of change ratios.

18. Again, a false-color composite of SAR images X_1 and X_3 is generated (Fig. 18d) and apparent changes are identified in optical images (Fig. 19). The reference data show that three walls of a building complex in the scene center (named building 6 below) are demolished. The walls are marked with red lines in Fig. 19.

In the segmentation step, 15 isolated buildings are extracted from the nDSM (see IDs in Fig. 22a) and further decomposed into wall segments. Building 6 is the largest building in the scene, resulting in 94 wall segments with individual IDs (see Fig. 20). The known demolished building segments are assigned with IDs 37, 48, and 80. GeoRaySAR is used to identify layover parts related to the building walls. Finally,

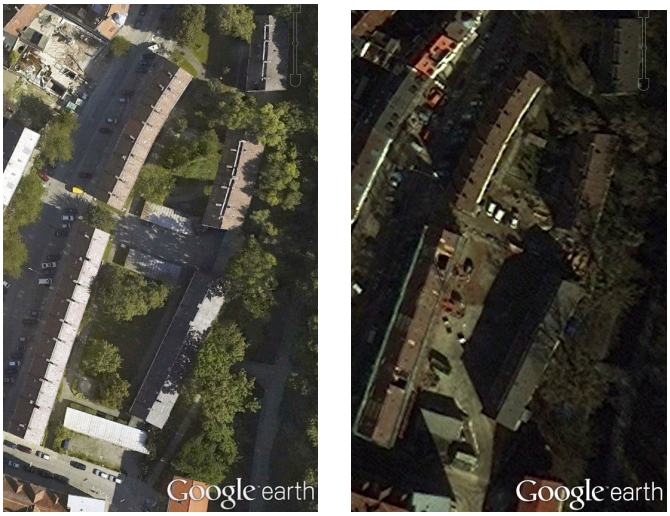

Fig. 17: Construction work related to building blocks 13 (bottom left) and 11 (two buildings in a row on the right). Left: image from 2007-08-25 (compare: TerraSAR-X image captured on 2008-06-27); Right: image from 2010-02-25 (compare: TerraSAR-X image captured on 2010-01-10). Top-left: reconstruction area R2.

the geometry of the layover areas is adapted based on the geometric projection described in section III-B1, followed by a comparison of the position of layover fill.

The derived change-ratio values for the 16 visible walls of building 6 range between 0.2 and 0.8. Fig. 21 shows the resulting change ratio map. The change ratios of wall segments 37, 48 and 80 are respectively 0.77, 0.63, and 0.62 for the WFP method, and are thus much higher than the change ratios of the other wall segments (compare Fig. 21). The separation of "change" and "no change" can be done the same way as for the BFR method based on the identification of gaps in the histogram of change ratios (see section IV-C and discussion in section V).

It should be noted that the change detection analysis may be affected by several factors. Due to the necessary layover projection, the WFP method is sensitive to the resolution of the DSM and the accuracy of the extracted wall parameters (wall center point position, wall gradient direction). Moreover, changes to roof structures or materials as well as neighboring buildings might affect the individual analysis of building walls. As an example, the high change ratio of wall 42 occurs due to the adjacent wall 48 and the resulting merged layover in the TerraSAR-X image. The demolition of wall 48 leads to a decreased intensity in the layover of wall 42 and triggers a high change ratio.

As a consequence, the decision for changes is combined into a building change ratio, using the wall layover areas as weights (see equation 12). With respect to the considered scene, the majority of buildings reveal change ratios between 0.3 and 0.4. Although only a small part of building 6 is changed, the resulting change ratio is much higher than for the other buildings (see Fig. 22a). For comparison, the change ratio based on the BFR method (on building level) is shown in Fig. 22b (see method in section III-A). As expected, the change

to building 6 appears less prominent compared to the other buildings, as that the change analysis is conducted for the building as a whole.

V. Discussion

Considering the results of the case study, the following strategy for change detection is recommended. The algorithm based on Building Fill Ratio (BFR), which analyzes building block changes, is suggested for detecting prominent building changes based on a DSM and two SAR images (acquired with equal or different signal incidence angles). It relies on one segmentation step, where the nDSM is decomposed into building models, and is much faster than the strategy based on individual wall models (increased number of input models). Moreover, a geometric projection sensitive to modeling errors is not required. Extended building changes are assigned with high change ratios. However, as shown by the histogram in Fig. 14, buildings with mid-level change ratios are likely to remain. For buildings with sufficient spatial extent in the SAR image, the algorithm based on the wall fill position (WFP) offers a complementary strategy to uncover partly changes. To this end, a further segmentation step is necessary to decompose building blocks into wall models. The focus on distinct building blocks is motivated by the increasing number of input models for the WFP method (see example in section IV-D: 16 wall models instead of 1 building model).

Facades are often characterized by prominent point signatures that are mostly related to corner structures, e.g., at windows or balconies. For good reasons, however, change detection based on variable signal incidence angles should not focus on these signatures in the first place. First, the assignment of point signatures to walls may be wrong as they may also correspond to roof / ground parts or even adjacent buildings mapped to the same position in the SAR image. Second, signal incidence angle variations often lead to the disappearance of prominent facade signatures due to a change of occlusion effects (e.g. corners hidden by facade structures or nearby buildings). The loss of signatures will result in false alarms. Third, the reliability of the change detection result depends on the number of distinguished point signatures, imposing a second criterion besides the visibility criterion to the wall. Finally, the assignment of point signatures based on the geometric projection will be even more sensitive to the accuracy of the wall model. Given the reasons above, it is recommended to integrate the analysis of salient signatures on a level beyond the WFP method in an opportunistic manner. If available, regularities can be considered as additional building hints [5], [34].

Further important aspects of the proposed change detection methodology can be summarized as follows:

- **Spatial resolution:** The algorithms have been developed in the context of meter resolution sensors, such as TerraSAR-X / TanDEM-X, and aim at a comprehensive analysis of urban scenes. As the methods primarily rely on areal indicators, the building size is the limiting factor. Accordingly, change detection may also be possible with medium resolution SAR images for extended building blocks.
- **Transferability to other scenes:** The applicability to other urban scenes is favored due to the fact that no scene-specific parameters are required for processing. Crucial factors with respect to the scene setting include the building size (impact on DSM segmentation), the variation of building materials (impact on threshold definition), and the density of objects (impact on layover areas corresponding to individual objects). As of yet, only the impact of small building sizes has been recognizable. This leads to a loss of building models during segmentation, whereas the other limits did not hamper our case studies.
- **Threshold definition:** The selection of thresholds for separating layover, ground, and shadow pixels requires moderate scene heterogeneity (in particular for buildings). The selection of a threshold for separating ”change” and ”no change” in the change ratio histogram is to be based on a compromise. For high correctness, the identification of prominent histogram gaps is recommended, which will lead to high thresholds and a restriction to extended changes. For high completeness, secondary gaps with lower values may be selected for thresholding. In this case, buildings with moderate changes will be included at the likely cost of an increase of the false alarm rate. In an automatic procedure, the threshold may be also determined, for instance, by the Expectation Maximization (EM) algorithm [35] in the case that sufficient samples are available for change and no change.
- **Difference in aspect angle:** The change analysis has to be conducted for the same building parts. That is, the SAR image pair has to be captured with the same node type (either both ascending or descending). Small differences to the azimuth angles, related to neighboring satellite orbits, are however covered for by considering the known heading angles during the simulation procedure.
- **Salient signatures:** Due to the presence of non-vertical walls in the 2.5D DSM, simulated corner lines located at the bottom of the facade are slightly shifted towards the interior of the layover (reason: building walls are slightly squinted towards the roof parts). For the DSM of our case study, this shift did not hamper the change analysis. Point and line signatures related to building floors are extracted based on the simulated layover extent. The impact of losing individual signatures due to incidence angle differences is attenuated by the concept of using areal change indicators. Nonetheless, large differences of incidence angles may hamper the comparability of building appearances and thereby the threshold definition.
- **Localization errors:** Both the simulated image layers and the real SAR images are related to the scene geometry (real shape, DSM). The images are matched by the projection on the same horizontal plane (frame mean height) where change detection is conducted. In this context, the extraction of the corresponding image parts depends on the accuracy of the DSM (e.g. based on LiDAR point cloud), the geocoded SAR images, and the assumption during the simulation step. However, the impact of the effects is negligible [23]. The projection

(a) TerraSAR-X image from 2008-05-26, incidence angle 25.3°

(b) TerraSAR-X image from 2010-01-05, incidence angle 39.3°

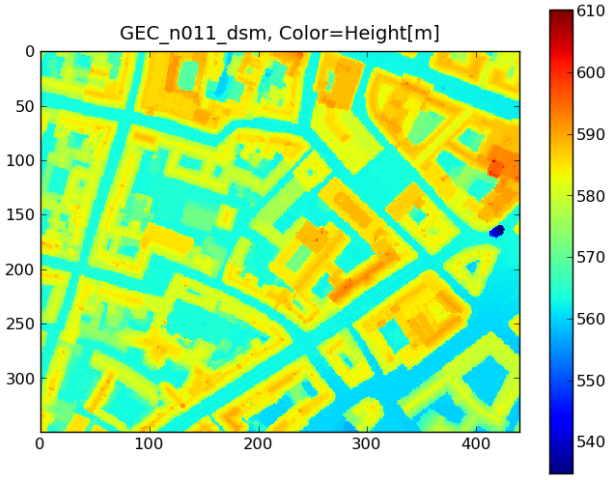

(c) DSM based on LiDAR data from April 2003

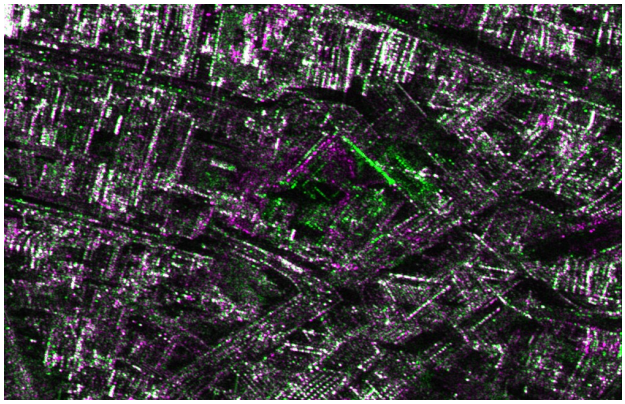

(d) Multi-temporal false color composite of spotlight TerraSAR-X images X_1 and X_3 (green channel: 2008-05-26, red and blue channel: 2010-01-10, both captured with incidence angle 25.3°). Magenta and green indicate increased and decreased intensity.

Fig. 18: Change detection on wall level: input data and false color composite.

on image planes leads to georeferencing errors as the elevation of buildings is neglected. However, changes detected by the methods are related to buildings or wall objects, which have world coordinates.

- **Slant-range geometry:** The analysis for changes may also be conducted based on SAR images in the azimuth-range plane using position annotations in the image meta data. However, a solution in this direction has not yet been pursued as the interfaces to other data formats would be blocked (e.g. optical or 3D GIS data).

Other sources of prior knowledge can also be integrated into the change detection procedure. 3D GIS data may be of particular interest in this context, e.g., using the open data model standard CityGML [36]. For instance, a solution to an interface between CityGML and GeoRaySAR is reported in [32]. In contrast to a DSM, GIS data can be updated frequently and, thus, differences between the geometric model and the pre-event reality may be minimized. Segmentation steps can be avoided. The accuracy of 3D vector models is higher than that of 2.5D segments extracted from a DSM. Accordingly, the impact of projection errors can be reduced. Most importantly, GIS data provide semantic information, removing the need for discriminating settlements from vegetation and segmentation steps. As a further advantage, the building type (e.g. residential, industrial) can be assigned to the detected change to support decision-makers in urgent situations.

VI. Conclusions and Outlook

Two fully-automatic, building-related change detection methods based on two high resolution SAR images and a digital surface model (DSM) have been presented in this paper for conducting the analysis on either the building level (building fill ratio, BFR) or wall level (wall fill position, WFP). The methods are based on geocoded simulated image layers for building / wall layover, shadow areas, and ground parts, which are directly superimposed on high resolution SAR images. Based on the integration of geometric prior knowledge from the DSM, change detection can be conducted on the building or facade level for equal or variable signal incidence angles. A case study for a test scene in Munich based on

Fig. 19: Apparent changes identified visually from Google Earth images. (top) 2007-08-25, (bottom) 2009-05-23. The demolished building parts are marked with colored polygons whereof the red lines denote demolished walls facing the SAR sensor.

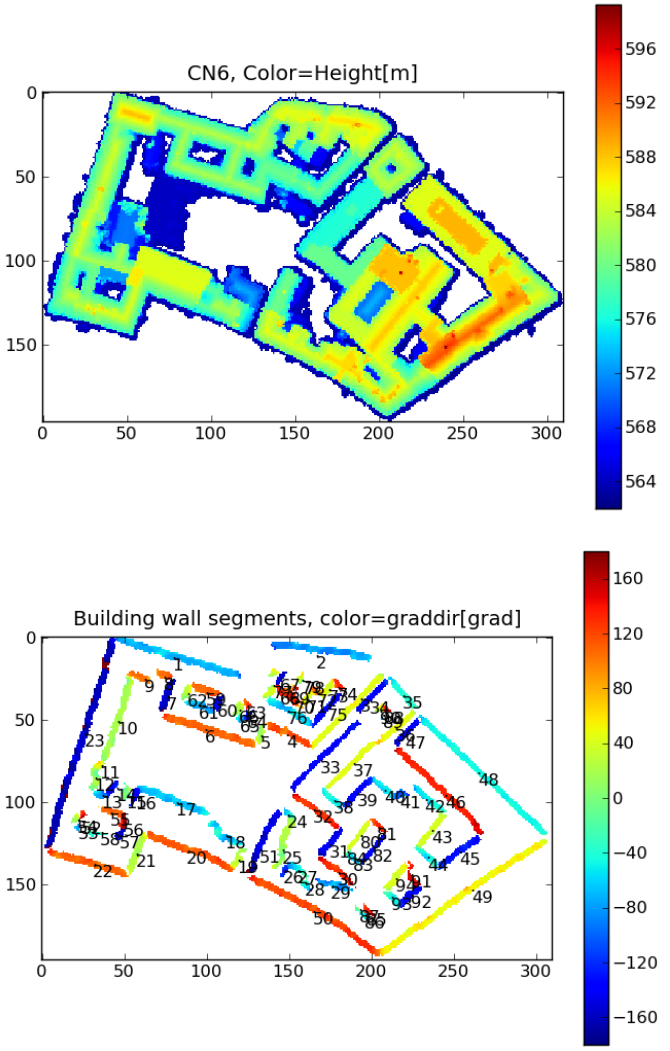

Fig. 20: Segmentation of Building 6; top: nDSM with color indicating height [m], bottom: wall segments with IDs with color indicating the gradient direction [°].

spotlight TerraSAR-X data and a DSM based on LiDAR data has been presented to confirm that BFR provides for the detection of prominent building block changes, whereas partly changed buildings can be highlighted based on the WFP method. A strategy for combining both methods has been presented and discussed, while also considering the limits of application.

Future work will concentrate on the integration of 3D GIS data, which is of high value due to its actuality, accuracy, and semantic information. Moreover, the development of advanced change indicators will be pursued.

REFERENCES

[1] W. Pitz and D. Miller, "The TerraSAR-X satellite," *IEEE Trans. Geosci. Remote Sens.*, vol. 48, no. 2, pp. 615–622, 2010.

[2] P. Lombardo, "A multichannel spaceborne radar for the COSMO-SkyMed satellite constellation," in *Proceedings of IEEE Aerospace Conference*, vol. 1, 2004, pp. 111–119.

[3] U. Stilla, "High resolution radar imaging of urban areas," in *Photogrammetric Week*, D. Fritsch, Ed., Stuttgart, 2007, pp. 149–158.

[4] E. Simonetto, H. Oriot, and R. Garello, "Rectangular building extraction from stereoscopic airborne radar images," *IEEE Trans. Geosci. Remote Sens.*, vol. 43, no. 10, pp. 2386–2395, 2005.

[5] E. Michaelsen, U. Soergel, and U. Thoennessen, "Perceptual grouping for automatic detection of man-made structures in high-resolution SAR data," *Pattern Recogn. Lett.*, vol. 27, no. 4, pp. 218–225, 2006.

[6] K. Goel and N. Adam, "Three-dimensional positioning of point scatterers based on radargrammetry," *IEEE Trans. Geosci. Remote Sens.*, vol. 50, no. 6, pp. 2355–2363, 2012.

[7] S. Gernhardt and R. Bamler, "Deformation monitoring of single buildings using meter-resolution SAR data in PSI," *ISPRS J. Photogramm. Remote Sens.*, vol. 73, pp. 68–79, 2012.

[8] X. Zhu and R. Bamler, "Very high resolution spaceborne SAR tomography in urban environment," *IEEE Trans. Geosci. Remote Sens.*, vol. 48, no. 12, pp. 4296–4308, 2010.

[9] J. Wegner, J. Ziehn, and U. Soergel, "Combining high-resolution optical and InSAR features for height estimation of buildings with flat roofs," *IEEE Trans. Geosci. Remote Sens.*, vol. 52, no. 9, pp. 5840–5854, 2014.

[10] S. Stramondo, C. Bignami, M. Chini, N. Pierdicca, and A. Tertulliani, "Satellite radar and optical remote sensing for earthquake damage detection: results from different case studies," *Int. J. Remote Sens.*, vol. 27, pp. 4433–4447, 2006.

[11] M. Chini, N. Pierdicca, and W. Emery, "Exploiting SAR and VHR

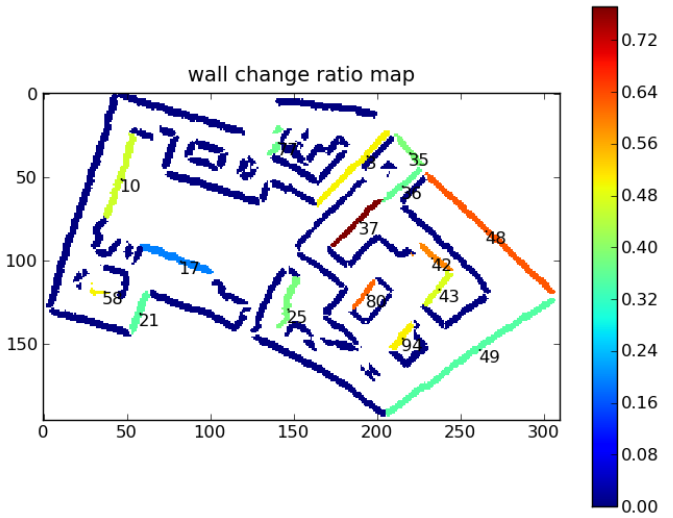

Fig. 21: Change ratio map based on the wall fill position (WFP method).

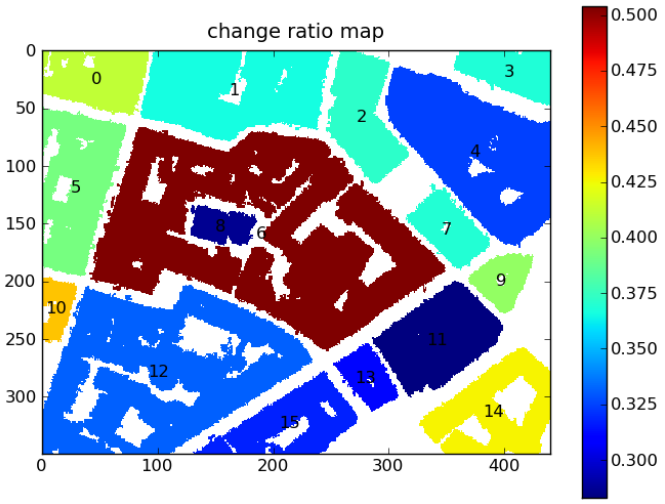

(a) Change ratio map based on wall fill position (WFP method)

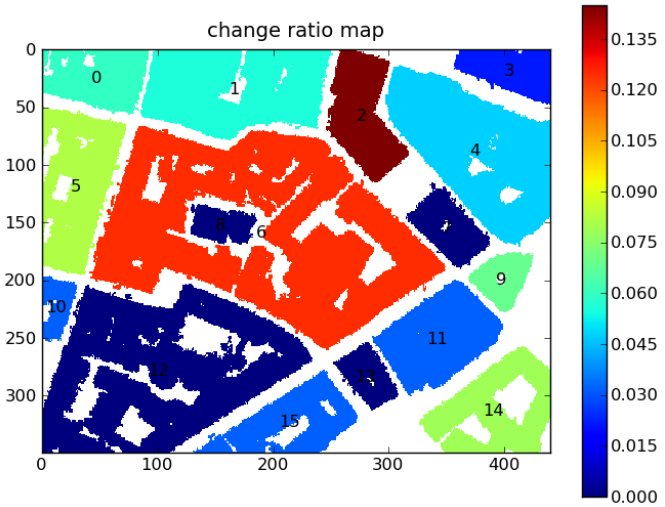

(b) Change ratio map based on building fill ratio (BFR method)

Fig. 22: Comparison of change detection results. Colors represent change ratios.

optical images to quantify damage caused by the 2003 Bam earthquake," *IEEE Trans. Geosci. Remote Sens.*, vol. 47, no. 1, pp. 145–152, 2009.

[12] E. Barthelet, G. Mercier, and L. Denise, "Building change detection in a couple of optical and SAR high resolution images," in *Proceedings of IGARSS*, 2011, pp. 2393–2396.

[13] N. Longbotham, F. Pacifici, T. Glenn, A. Zare, M. Volpi, D. Tuia, E. Christophe, J. Michel, J. Inglada, J. Chanussot, and Q. Du, "Multi-modal change detection, application to the detection of flooded areas: Outcome of the 2009-2010 data fusion contest," *IEEE J. Sel. Topics Appl. Earth Observ. in Remote Sens.*, vol. 5, no. 1, pp. 331–342, 2012.

[14] U. Soergel, U. Thoennessen, A. Brenner, and U. Stilla, "High-resolution SAR data: new opportunities and challenges for the analysis of urban areas," *IEE Proceedings - Radar, Sonar and Navigation*, vol. 153, no. 3, pp. 294–300, 2006.

[15] A. Schmitt, B. Wessel, and A. Roth, "Curvelet approach for SAR image denoising, structure enhancement, and change detection," in *International Archives of Photogrammetry, Remote Sensing and Spatial Information Sciences*, vol. 38-3/W4, 2009, pp. 151–156.

[16] F. Bovolo, C. Marin, and L. Bruzzone, "A hierarchical approach to change detection in very high resolution SAR images for surveillance applications," *IEEE Trans. Geosci. Remote Sens.*, vol. 51, no. 4, pp. 2042–2054, 2013.

[17] D. Brunner, G. Lemoine, and L. Bruzzone, "Earthquake damage assessment of buildings using VHR optical and SAR imagery," *IEEE Trans. Geosci. Remote Sens.*, vol. 48, no. 5, pp. 2403–2420, 2010.

[18] C. Marin, F. Bovolo, and L. Bruzzone, "Building change detection in multitemporal very high resolution SAR images," *IEEE Trans. Geosci. Remote Sens.*, vol. 53, no. 5, pp. 2664–2682, 2015.

[19] F. Dell'Acqua and P. Gamba, "Remote sensing and earthquake damage assessment: Experiences, limits, and perspectives," *Proceedings of the IEEE*, vol. 100, no. 10, pp. 2876–2890, 2012.

[20] T. Balz, "SAR simulation based change detection with high-resolution sar images in urban environments," in *Proceedings of ISPRS congress*, vol. 35, Part B, 2004.

[21] T. Wang and Y. Jin, "Postearthquake building damage assessment using multi-mutual information from pre-event optical image and postevent SAR image," *IEEE Geosci. Remote Sens. Lett*, vol. 9, no. 3, pp. 452–456, 2012.

[22] H. Arefi, P. d Angelo, H. Mayer, and P. Reinartz, "Iterative approach for efficient digital terrain model production from CARTOSAT-1 stereo images," *J. Appl. Remote Sens.*, vol. 5, no. 1, pp. 053 527–053 527–19, 2011.

[23] J. Tao, S. Auer, G. Palubinskas, P. Reinartz, and R. Bamler, "Automatic SAR simulation technique for object identification in complex urban scenarios," *IEEE J. Sel. Topics Appl. Earth Observ. in Remote Sens.*, vol. 7, no. 3, pp. 994–1003, 2014.

[24] S. Auer, S. Hinz, and R. Bamler, "Ray-tracing simulation techniques for understanding high-resolution SAR images," *IEEE Trans. Geosci. Remote Sens.*, vol. 48, no. 3, pp. 1445–1456, 2010.

[25] H. Hammer and K. Schulz, "Coherent simulation of SAR images," in *Proceedings of SPIE Image and Signal Processing for Remote Sensing XV*, vol. 7477, 2009.

[26] T. Balz and U. Stilla, "Hybrid GPU-based single- and double-bounce SAR simulation," *IEEE Trans. Geosci. Remote Sens.*, vol. 47, pp. 3519–3529, 2009.

[27] S. Auer and S. Gernhardt, "Linear signatures in urban SAR images - partly misinterpreted?" *IEEE Geosci. Remote Sens. Lett*, vol. 10, pp. 1762–1766, 2014.

[28] P. Brett and R. Guida, "Earthquake damage detection in urban areas using curvilinear features," *IEEE Trans. Geosci. Remote Sens.*, vol. 51, no. 9, pp. 4877–4884, 2013.

[29] A. Ferro, D. Brunner, and L. Bruzzone, "Automatic detection and reconstruction of building radar footprints from single VHR SAR images," *IEEE Trans. Geosci. Remote Sens.*, vol. 51, no. 2, pp. 935–952, 2013.

[30] C.-A. Deledalle, L. Denis, and F. Tupin, "Iterative weighted maximum likelihood denoising with probabilistic patch-based weights," *IEEE Trans. Image Process.*, vol. 18, no. 12, pp. 266–272, 2009.

[31] C. Oliver and S. Quegan, *Understanding Synthetic Aperture Images*. SciTech Publishing, Inc., 2004.

[32] S. Auer and A. Donaubauer, "Buildings in high resolution SAR images - identification based on CityGML data," in *Proceedings of Photogrammetric Image Analysis (PIA) Conference*, 2015.

[33] S. Auer, S. Gernhardt, and R. Bamler, "Ghost persistent scatterers related to multiple signal reflections," *IEEE Geosci. Remote Sens. Lett*, vol. 8, no. 5, pp. 919–923, 2011.
[34] S. Auer, C. Gisinger, and J. Tao, "Characterization of facade regularities in high-resolution SAR images," *IEEE Trans. Geosci. Remote Sens.*, vol. 53, no. 5, pp. 2727–2737, 2015.
[35] L. Bruzzone and D. Prieto, "Automatic analysis of the difference image for unsupervised change detection," *IEEE Trans. Geosci. Remote Sens.*, vol. 38, pp. 1171–1182, 2000.
[36] G. Groeger, T. H. Kolbe, C. Nagel, and K.-H. Haefele, *OGC City Geography Markup Language (CityGML) Encoding Standard, v2.0. OGC Doc. No. 12-019*. Open Geospatial Consortium, 2012.

Junyi Tao was born in Wuhan, P.R.China, in 1983. He received the Dipl.-Ing.(Univ.) degree in Geodesy and Geoinformatics from the Universität Stuttgart, Germany, in 2009, and the Dr.-Ing. degree in Geodesy and Geoinformatics from Technische Universität München, Munich, Germany, in 2015. From October 2009 to 2014, he was a scientific collaborator with the Remote Sensing Technology Institute (IMF), German Aerospace Center (DLR), Oberpfaffenhofen, Germany, working in close cooperation with the chair of Remote Sensing Technology (LMF), Technische Universität München (TUM), Munich, Germany. In June 2012, he was a guest scientist at the Remote Sensing Laboratory, Department of Information Engineering and Computer Science, University of Trento, Trento, Italy. He pursued research topics in the field of SAR simulation, SAR image interpretation, multi-modal data fusion, and change detection. In particular, he focused on the combination of LiDAR and SAR data with simulation techniques for object identification and change detection in urban areas. Currently, he is working in the R&D Department of a privately held company, where he is further developing his expertise in sensor data fusion.

Dr. Tao was the recipient of the second prize in the IEEE GRSS Data Fusion Contest in 2012, together with Stefan Auer and Richard Bamler from TUM/DLR.

Stefan Auer received the Dipl.-Ing.(Univ.) degree in Geodesy in December 2005 and the Dr.-Ing. degree in April 2011, both from the Technische Universität München (TUM). After moving from TUM in December 2014, he is senior scientist and project manager at the Remote Sensing Technology Institute (IMF), German Aerospace Center (DLR), Oberpfaffenhofen, Germany. Besides projects in the field of optical and hyperspectral imaging, he is concerned with the understanding and analysis of SAR imagery.

In the course of his doctoral thesis, Stefan Auer spent three months as guest researcher at the Department of Electronic and Telecommunication Engineering (DIET) at the University of Naples "Federico II" in Italy.

His main interest is in the visual and automated interpretation of high resolution SAR images and in the evaluation of the 3D localization capability of interferometric SAR algorithms. In this context, Stefan Auer developed the 3D SAR simulator RaySAR which enables to investigate the nature of prominent SAR image signatures corresponding to man-made structures. Based on the knowledge from simulation case studies, he is also working on algorithms for characterizing signature regularities related to building facades.